

# UOD: Unseen Object Detection in 3D Point Cloud

Hyunjun Choi<sup>1,2\*</sup> Daeho Um<sup>1</sup> Hawook Jeong<sup>2</sup>

<sup>1</sup> ASRI, ECE., Seoul National University <sup>2</sup> RideFlux Inc.

numb7315@snu.ac.kr daehoum1@snu.ac.kr hawook@rideflux.com

Existing 3D object detectors encounter extreme challenges in localizing unseen 3D objects and recognizing them as unseen, which is a crucial technology in autonomous driving in the wild. To address these challenges, we propose practical methods to enhance the performance of 3D detection and Out-Of-Distribution (OOD) classification for unseen objects. The proposed methods include anomaly sample augmentation, learning of universal objectness, learning of detecting unseen objects, and learning of distinguishing unseen objects. To demonstrate the effectiveness of our approach, we propose the KITTI Misc benchmark and two additional synthetic OOD benchmarks: the Nuscenes OOD benchmark and the SUN-RGBD OOD benchmark. The proposed methods consistently enhance performance by a large margin across all existing methods, giving insight for future work on unseen 3D object detection in the wild.

## 1. Introduction

In autonomous driving scenarios, 3D object detection using point clouds is a crucial perception technology. The recognition performance of 3D object detectors has advanced under the closed-world assumption, but there are two issues regarding stability in open-world scenarios: whether they can detect unseen objects and differentiate them as unseen objects. In first issue, methods addressing open-world 2D object detection [12, 14] or instance segmentation [19] have tackled issues in 2D images. However, there are still uncertainties regarding 3D point clouds. In the second issue, methods addressing Out-of-Distribution (OOD) detection [4, 5] for 2D object detection on images have tackled similar challenges. Similarly, in the realm of 3D object detection [2, 11, 25] on point clouds, efforts are underway to address these issues, but they only focus on the classification of unseen objects. Detection of unseen objects is a prerequisite preceding classification for safety in autonomous driving. In this paper, the term ‘OOD classification’ will replace the conventional term ‘OOD detection’.

We have found that recent 3D object detectors [15, 20, 21, 26] face challenges in detecting unseen objects in open-

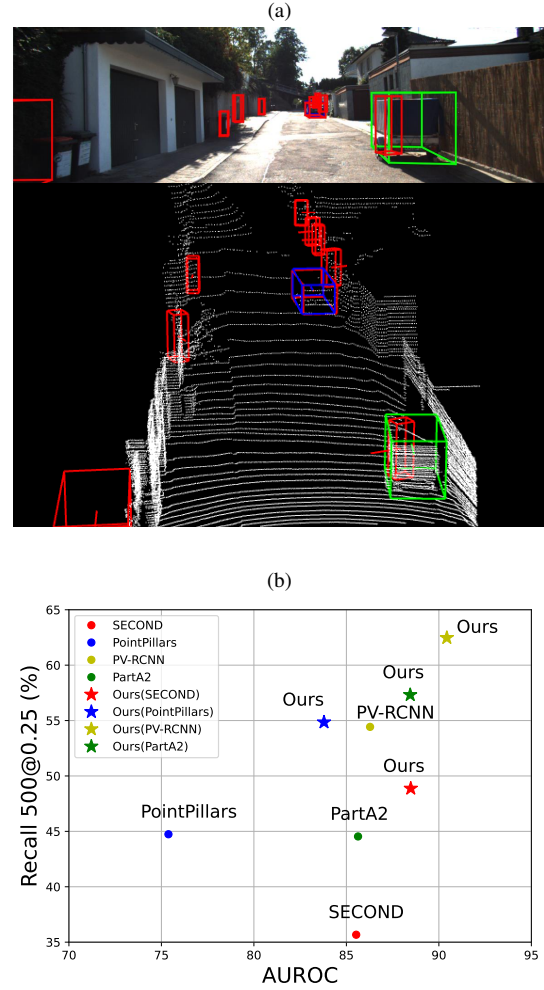


Figure 1. **Base 3D object detector and our method comparison.** (a): 3D object detection result of baseline SECOND [26] on KITTI [6] ‘Misc’ class object; (b): Comparison of the base detector and our method in two aspects: unseen object detection performance (Recall) and OOD classification performance (AUROC).

world scenarios. Specifically, unlike 2D images, for the 3D detection of unseen objects, Lidar point clouds are sparse, making it challenging to obtain accurate context and precisely localize unseen objects with various sizes. As depicted in Figure 1a, a SECOND [26] detector, which is trained on the classes of Car, Pedestrian, and Cyclist, fails to localize the ‘Misc’ class object within the green box even at a close distance. Instead, SECOND recognizes the unseen object as a smaller pedestrian, leading to significant failures in 3D localization. Furthermore, addressing localization issues is a crucial prerequisite for OOD classification. If the detector fails to localize an unseen object, obtaining its detection results and classifying it as an unseen object becomes impossible. Therefore, in open-world scenarios, it is essential to evaluate not only the OOD classification but also their detection performance.

In this paper, we address the open-world 3D object detection problem through two main directions: (i) introducing an integrated protocol for evaluating the safety of 3D object detectors, and (ii) presenting methodologies for enhancement. We propose a comprehensive protocol for evaluating open-world 3D object detection, assessing both the detection of unseen objects and their OOD classification, simultaneously. Our ideal 3D object detector excels in precisely localizing unseen objects while assigning high OOD confidence scores to them. As in previous open-world object detection [14], the detection performance is measured by the recall of unseen objects at multiple IOU thresholds. OOD classification utilizes conventional base metrics: AU-ROC, FPR, and AUPR.

In line with our integrated 3D detector evaluation protocol, we propose methods to simultaneously enhance unseen object detection and OOD classification performance. We introduce an anomaly sample augmentation approach inspired by the outlier exposure method [9], acquiring anomaly samples from indoor scene SUN-RGBD [22] data and incorporating them as a new additional class for training. As a result, our method undergoes training to detect unseen objects of various sizes. Next, we address the conflicting aspects between unseen object detection and OOD classification. In the structure of existing 3D detectors, assigning low In-Distribution (ID) confidence scores to unseen objects is inherently linked to assigning low objectness scores for unseen objects. We need to assign low In-Distribution (ID) confidence scores to unseen objects while assigning high objectness scores for detection. Therefore, we add a separate objectness node alongside the classification nodes for the 3D object detector. In addition to the proposed augmentation, we introduce a novel technique to enhance OOD classification performance by leveraging energy-based regularization and outlier-aware supervised contrastive learning using the anomaly samples introduced in the proposed augmentation. As evident from Figure 1b, the application of

our methods yields improvements in both the detection and OOD classification of unseen objects compared to the four baseline detectors.

Practically, we measure unseen object detection and OOD classification on Lidar-based detectors trained on KITTI [6] scenes. We designate the ‘Misc’ class as the unseen object, creating the KITTI Misc benchmark, and propose baselines for four existing detectors: SECOND [26], PointPillars [15], PV-RCNN [21], and PartA2 [20]. Moreover, to assess safety for a more diverse range of unseen objects, we propose two additional benchmarks: the Nuscenes [1] OOD benchmark and the SUN-RGBD [22] OOD benchmark. We introduce various new unseen objects from large-scale outdoor scenes Nuscenes and indoor scenes SUN-RGBD into the outdoor scene of KITTI.

In summary, our contribution can be outlined as follows:

- (i) Introducing an integrated protocol for evaluating open-world 3D object detection on KITTI scenes, providing baseline assessments for four 3D object detectors: SECOND, PointPillars, PV-RCNN, and PartA2.
- (ii) Applying practical methods enhances open-world 3D object detection performance in both unseen object detection and OOD classification from existing 3D object detector baselines.
- (iii) Constructing three benchmark scenarios to model a diverse range of unseen objects and confirming our method’s significant improvement over baselines

## 2. Related Work

### Unseen Object Detection in Open-world

Unseen object detection has primarily been tackled within the realm of 2D object detection under the open-world assumption. [14] advanced universal unseen object detection by omitting classification nodes within the region proposal network of 2D object detectors. [12] refines unseen object detection within open-world contexts through incremental learning of unseen objects. [19] endeavors to enhance unseen object detection by substituting unannotated objects with annotated objects via augmentation in the instance segmentation task. While existing works have addressed unseen object detection for 2D images, we have discovered significant challenges in 3D object detection on 3D point clouds and have made substantial improvements in this regard.

### OOD detection on Object Detection

In recent 2D object detection, the STUD [4] and VOS [5] papers introduced OOD classification tasks. They measure the OOD classification performance by distinguishing scenes with only known (seen) objects and scenes without them, considering all scores obtained from the detector. However, these methods deal only with 2D images and may not be practical as they are not suitable for many real-world environments where known (seen) and unknown (unseen) objects coexist. Recently, in Lidar-based 3D object detec-

tion, an OOD classification task has been proposed in [11] that aimed to evaluate OOD classification when known (seen) and unknown (unseen) instances coexist. However, this method solely focuses on OOD object dataset generation without improving performance. Similarly, 3D Open-set object detection [2] aimed to improve detection accuracy when known and unknown instances coexist. However, due to the different metrics, direct comparisons become difficult, and unlike using heuristics to distinguish unknown instances, we provide a heuristic-free clear evaluation.

### Lidar-based 3D Object Detection

3D object detection based on Lidar point clouds has seen significant improvement by aggregating features through voxel-based learning [27]. SECOND [26] enhances speed over VoxelNet [27] by replacing its conventional 3D convolution with sparse convolution. PointPillars [15] divides the point cloud into pillar units and applies PointNet to each unit. In contrast to SECOND and VoxelNet, which use 3D convolution to integrate voxel units, PointPillars uses 2D convolution to integrate pillar units which boosts efficiency in time. PartA2 [20] newly designs a RoI-aware point cloud pooling module to encode effective features of 3D proposals. PV-RCNN [21] extends SECOND, preserving more 3D structure information by adding a keypoint branch. Existing methods have primarily focused on improving detection precision in closed environments. However, there has not been a clear investigation into the ability of 3D object detectors in open-world scenarios to detect and differentiate unseen objects.

## 3. 3D Open-World Object Detection

### 3.1. Problem Formulation and Evaluation

We can formalize a Lidar-based 3D object detector that maps a point cloud consisting of  $M$  points to  $N$  detected objects as  $\mathbf{z}(\mathbf{x}) : \mathbb{R}^{D \times M} \rightarrow \mathbb{R}^{L \times N}$ , where  $D$  denotes the dimension of a point including location  $(x, y, z)$  and  $L$  denotes the dimension of detection results. Object detection results consist of  $N$  detected objects  $\{O_1, \dots, O_N\}$  where  $O_i = \{conf_i, \mathbf{c}_i, x_i, y_i, z_i, l_i, w_i, h_i, \theta_i\}$ . Here,  $conf_i$  is defined as the final objectness score, representing the degree to which an object is present. A classification score with a total of  $K$  classes is defined as  $\mathbf{c}_i = [c_1, c_2, \dots, c_K]^T$ . The set  $\{x_i, y_i, z_i, l_i, w_i, h_i, \theta_i\}$  corresponds to the 3D detection box, defined as a cuboid with an orientation angle.

In practical terms, to address the unseen object detection problem, we utilize a detector that identifies three classes in the KITTI dataset [6], including car, pedestrian, and cyclist (i.e.,  $K = 3$ ). For unseen objects, we define the ‘Misc’ class provided in the actual KITTI dataset. We refer to this as the KITTI Misc benchmark and propose a protocol for its evaluation. In the evaluation, we simultaneously assess two aspects of unseen objects: unseen object detection and OOD

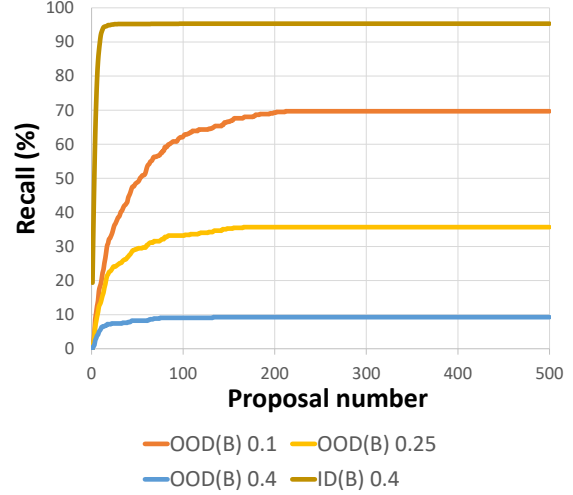


Figure 2. **In-Distribution (ID)(seen) and Out-Of-Distribution (OOD)(unseen) object localization performance comparison.** This plot illustrates the recall for both ID (seen) and OOD (unseen) objects based on the proposal number. This depicts the recall for OOD objects at IoU thresholds of 0.1, 0.25, and 0.4.

classification. For localization, we utilize  $conf_i$ . For OOD classification, we obtain scalar scores (e.g., MSP [8], Energy [17]) from  $\mathbf{c}_i$  for evaluation. Unless stated otherwise, we use Energy score [17] for evaluation in this paper.

#### 3.1.1 Evaluation of Unseen Objects Detection

Generally, recall is a crucial metric for ensuring the safety of an object detector. As in previous open-world object detection studies [14], localization performance on OOD objects can be measured by recall. In actual KITTI settings, detectors often follow a base setting, obtaining a maximum of 500 results. We demonstrate recall results for the actual SECOND detector on KITTI as described in Fig 2. Specifically, recall is measured based on the proposal number and IOU threshold criteria. The predictions are uniformly restricted to the top- $k$  based on the score  $conf_i$  and similarly found based on the IOU threshold, calculating True Positives (TP) for objects predicted among actual objects, and then computing  $Recall = \frac{TP}{TP+FN}$ . As evident from the graph, the baseline detector, SECOND, significantly lags behind in OOD localization compared to ID at the same threshold of 0.40. Furthermore, our recall in the graph shows minimal differences beyond a proposal number of 300. Therefore, we fix the proposal number  $k = 500$  and evaluate localization performance based on three IOU thresholds: 0.10, 0.25, and 0.40.

### 3.1.2 Evaluation of OOD Classification

We obtain scores of object instances from the detection results where there is overlap, following the approach of OOD classification in the existing methods for both 2D object detectors [4, 5] and 3D object detectors [11]. Detailed algorithms are covered in the supplementary material. Subsequently, we adhere to the baseline method [8] for OOD classification in conventional image classification tasks. The evaluation metrics include AUROC, FPR95, and AUPR.

## 3.2. Proposed Method

Baseline 3D object detectors struggle with the detection and OOD classification of unseen objects. To address this, we employ two key strategies. First, inspired by outlier exposure [9], we introduce auxiliary unseen object data by copying and pasting from SUN-RGBD [22] indoor scenes, treating it as a new ‘Anomaly’ class for training unseen object detection across various sizes. Figure 3a illustrates this sample from SUN-RGBD. Second, to boost the OOD classification performance of baseline detectors, we utilize the Anomaly-class data to apply energy-based regularization and outlier-aware contrastive learning. Our approach consists of four main techniques: (i) Anomaly Sample Augmentation, (ii) Learning on Objectness, (iii) Learning on Localizing Unseen Objects, and (iv) Learning on Distinguishing Unseen Objects.

### 3.2.1 Anomaly Sample Augmentation

In the existing SECOND, the augmentation method during training involves sampling ground truths from the database, specifically copying object points and labels from the ground truth to training point clouds while checking for collisions to prevent unrealistic outcomes. We adopt a similar strategy for Anomaly Sample augmentation, constructing a database from SUN-RGBD data. From this database, we obtain anomaly samples using a copy-paste approach, treating them as an additional class (‘Anomaly’) for detector training. Anomaly Sample Augmentation trains the detector to localize unseen objects of various sizes or contexts. Specifically, we directly utilize the database formed in previous research [18] for indoor 3D object detection, which consists of 3D cuboids and their corresponding RGB-D point clouds.

### 3.2.2 Learning of Universal Objectness

Existing 3D object detectors often have a high correlation between classification scores and confidence scores. For instance, in a single-stage detector like SECOND, the confidence score  $conf_i$  operates as  $\max\{c_1, c_2, \dots, c_k\}$ . However, we aim to enhance unseen object detection and OOD classification separately. Therefore, we propose the addition

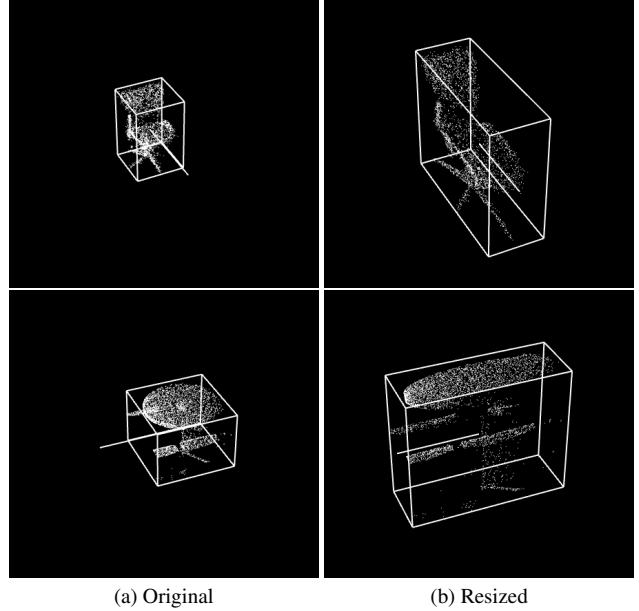


Figure 3. **Visualization result on SUN-RGBD [22] pointcloud of original and resized object.** (a): Point cloud of the original object for Anomaly Sample Augmentation; (b): Point cloud of the resized object for Multi-size Mix Augmentation.

of a separate objectness node that is trained for decoupling these aspects.

$$FL(p_t) = -\alpha(1 - p_t)^\gamma \log(p_t), \quad (1)$$

We use the conventional Focal loss employed in RetinaNet [16] with the established SECOND settings, setting  $\alpha = 0.25$  and  $\gamma = 2$ . We label the foreground, including the ID class and the ‘Anomaly’ class, as 1, and everything else as 0. The objectness loss constructed with Focal loss is denoted as  $L_{obj}$ . The introduced objectness node aims to model a universal objectness, akin to FasterRCNN [7]’s Region Proposal Network. In a single-stage detector, it serves as the confidence score, while in a two-stage detector, it acts as a bridge, forming proposals for subsequent stages. The final confidence score for the two-stage detector is derived through the second-stage classifier.

### 3.2.3 Learning of Detecting Unseen Objects

We train the model to detect objects of various sizes by adding the ‘Anomaly’ class with Anomaly Sample augmentation. However, as shown in Figure 3a, the sizes of indoor scene data are generally smaller or less diverse compared to outdoor scenes. To address this, we propose Multi-size Mix augmentation to create a more diverse set of anomaly objects. As illustrated in Figure 3b, we construct a database by resizing the original anomalies to various sizes and mixing them together. Specifically, Multi-size mix augmenta-



tion combines equal parts of the original anomaly at its original size and the resized anomaly. Additionally, the sizes for resizing the boxes are randomly extracted from various samples of box sizes in the KITTI Misc class.

### 3.2.4 Learning of Distinguishing Unseen Objects

The straightforward application of the previous simple OE loss is not effective when using Anomaly data for a one-vs-rest classifier. This is because the basic classifier already trains an additional Anomaly class as it should go to all zero for the existing In-Distribution (ID)(seen) classes. Therefore, we address this issue by introducing energy regularization loss [17], Furthermore, we enhance performance by incorporating outlier-aware contrastive learning [3], which improves the separability between In-Distribution (ID) and Out-Of-Distribution (OOD) data in the representation. Energy regularization loss is defined by

$$\begin{aligned} L_{en} &= L_{in,hinge} + L_{out,hinge} \\ &= \mathbb{E}_{(\mathbf{x}_{in}, y) \sim D_{in}^{train}} [(\max(0, E(\mathbf{x}) - m_{in}))^2] \\ &\quad + \mathbb{E}_{\mathbf{x} \sim D_{out}^{train}} [(\max(0, E(\mathbf{x}) - m_{out}))^2]. \end{aligned} \quad (2)$$

Here,  $D_{out}^{train}$  is defined as an 'Anomaly' class object. where  $E(\mathbf{x}; f) = -T \cdot \log(\sum_{j=1}^K e^{f_j(\mathbf{x})}/T)$ . Energy function  $E(\mathbf{x}; f)$  is computed as LogSumExp of logit with temperature scaling, In our cases, temperature  $T=1$ . Energy regularization loss is the sum of squared hinge losses for energy with each of the existing ID data and the auxiliary OOD ('Anomaly' class) data.

The loss for contrastive learning is defined by

$$L_c = \sum_{i \in B_{in}} L_i, \quad (3)$$

$$L_i = -\frac{\mathbf{1}_{\{|B_{y_i}^{in}| > 1\}}}{|B_{y_i}^{in}| - 1} \sum_{p \in B_{y_i}^{in} \setminus \{i\}} \log \frac{\exp(\tilde{\mathbf{f}}_i \cdot \tilde{\mathbf{f}}_p / \tau_c)}{\sum_{k \in B^{all} \setminus \{i\}} \exp(\tilde{\mathbf{f}}_i \cdot \tilde{\mathbf{f}}_k / \tau_c)}, \quad (4)$$

where we set  $\frac{\mathbf{1}_{\{|B_{y_i}^{in}| > 1\}}}{|B_{y_i}^{in}| - 1} = 0$  when  $|B_{y_i}^{in}| = 1$ ;

$\mathbf{1}_{\{|B_{y_i}^{in}| > 1\}} = 1$  when  $|B_{y_i}^{in}| > 1$ .

Within the total batch  $B^{all}$ , an instance  $\mathbf{x}_i$  holds the following representation  $\tilde{\mathbf{f}}_i$ .  $B^{all}$  has partition  $B^{in}$  and  $B^{out}$ , each of which is an ID object and an Anomaly class object, respectively.  $B_{y_i}$  is a subset of the set  $B$  where the label of every sample in  $B_{y_i}$  matches  $y_i$ . Outlier-aware contrastive learning takes into account outlier data in addition to the traditional supervised contrastive learning (SCL) [13]. As a result, total loss  $L_{total}$  for our loss is defined by

$$L_{total} = L_{cls} + L_{reg} + L_{obj} + \lambda_{en} L_{en} + \lambda_c L_c. \quad (5)$$

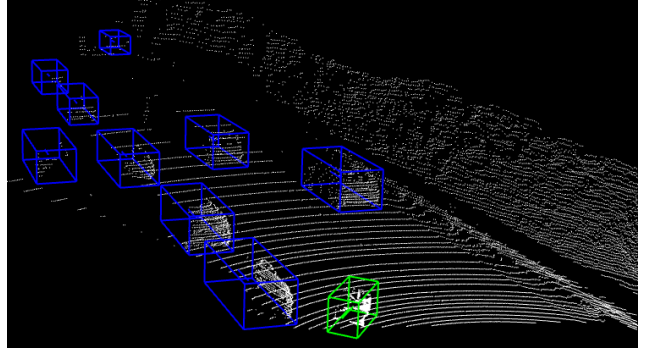


Figure 4. **Visualization on our proposed synthetic benchmark.** The blue box represents the original ID (seen) object, while the green box represents our cut-pasted synthesized OOD (unseen) object.

### 3.3. Additional Synthetic OOD Benchmark

Aiming to create scenarios with a more diverse range of unseen objects than KITTI's 'Misc' class, we further propose two additional synthetic OOD benchmarks by inserting instances of unseen object point clouds from external data into KITTI scenes using the cut-paste technique. This enables us to incorporate a wider variety of unseen objects into the benchmark. As depicted in Figure 4, our benchmark involves adding unseen objects to existing scenes. Blue represents the original in-distribution (seen) data, while green depicts the copy-pasted unseen objects. We aim to evaluate unseen object detection and OOD classification for existing baseline 3D detectors in scenes where these coexist.

Firstly, we propose the Nuscenes [1] OOD benchmark by extracting unseen object point cloud instances from the large-scale outdoor dataset, Nuscenes. We select a total of five unseen object classes: Debris, Pushable Pullable Object, Traffic Barrier, Traffic Cone, and Animal, which correspond to objects not typically seen in KITTI scenes. For each class, we propose a total of five benchmarks each representing a different unseen object scenario.

Secondly, we propose the SUN-RGBD [22] OOD benchmark by extracting unseen object point cloud instances from the indoor dataset, SUN-RGBD. Objects in SUN-RGBD indoor scenes are naturally unseen in the outdoor KITTI dataset. We compose a set of unseen objects using the remaining five classes from SUN-RGBD that are not used for training. However, due to the relatively small number of object instances in SUN-RGBD point clouds, we propose a single benchmark scenario that uses all five classes. More detailed methods for constructing challenging benchmarks are described in the supplementary material.

## 4. Experimental Result

### 4.1. Experiment Settings

We conduct experiments on the KITTI [6] training and validation sets with a 5:5 split. For the baseline configuration, the baseline detector is trained based on the code of OpenPCDet [23]. The key difference is that, in the training set, classes other than Car, Pedestrian, and Cyclist (e.g., Truck, Van, etc.) were removed from the point cloud to avoid training them as background. Also, we consistently aim to obtain a maximum of 500 detection results. For this purpose, SECOND and PointPillar maintain their original configuration settings from OpenPCDet. For PV-RCNN and PartA2, we changed the settings for inference in the first stage, increasing the NMS configuration of pre-max size to 8196 and post-max size to 2048 to ensure a lot of detection results. We utilized the  $\{R, G, B, x, y, z\}$  information from the SUN-RGBD dataset and followed the processing protocol outlined in [22] and [18]. The RGB values were averaged to convert them into intensity  $\{I, x, y, z\}$ , forming a 4D vector as same as KITTI.

For the KITTI Misc benchmark, we used the existing validation set but selected only scenes with Misc objects within the 0-50m distance range. From each scene where unseen objects coexist with seen objects, we collected OOD samples and ID samples for use in OOD classification. The recall was also measured by aggregating these scenes to evaluate unseen object recall. This is the same setting for a synthetic benchmark. Detailed hyperparameter settings and training environments are described in the supplementary material.

### 4.2. Evaluation on KITTI Misc benchmark

#### 4.2.1 Quantitative Result

We first quantitatively validate our method on the KITTI Misc benchmark, particularly showcasing superior localization performance for the Misc class, compared to the prominent baseline, SECOND. As depicted in Figure 5, regardless of proposal number and IOU thresholds (0.1, 0.25, 0.40), our method consistently exhibits excellent recall.

#### 4.2.2 Comparison with baseline

Our method goes beyond SECOND and evaluates unseen object detection (recall) and OOD classification performance for four detectors: SECOND, PointPillars, PV-RCNN, and Part-A2. As summarized in Table 1, the two-stage detectors, PV-RCNN and Part-A2, outperform single-stage detectors (PointPillars and SECOND) in both unseen object detection and OOD classification. Our method significantly improves recall and OOD detection across all detectors, as shown in Figure 1 of Introduction.

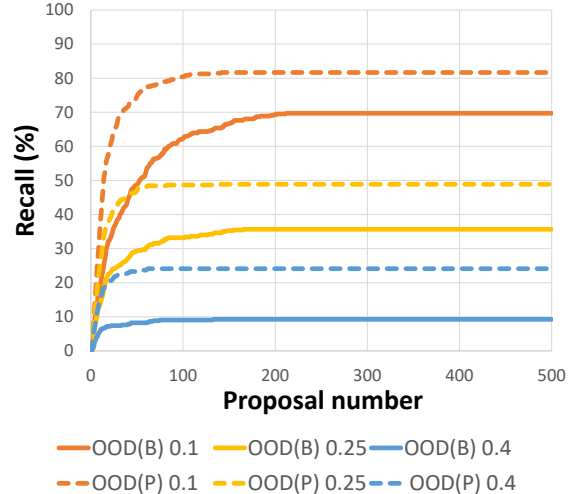


Figure 5. **OOD (unseen) object recall comparison on KITTI Misc benchmark.** OOD(B) represents the result of the baseline detector SECOND, and OOD(P) represents the result of our method on SECOND.

Table 1. Quantitative result of our method on KITTI Misc benchmark. 500 proposals are used for all cases.

METHOD		Recall @IOU			OOD detection		
		0.10	0.25	0.40	AUC $\uparrow$	AP $\uparrow$	FPR $\downarrow$
SECOND	Base	69.69	35.67	9.28	85.53	81.17	78.14
	<b>Ours</b>	<b>81.65</b>	<b>48.87</b>	<b>24.12</b>	<b>88.48</b>	<b>82.94</b>	<b>55.05</b>
PointPillars	Base	76.70	44.74	18.14	75.38	68.79	89.48
	<b>Ours</b>	<b>82.89</b>	<b>54.85</b>	<b>26.60</b>	<b>83.79</b>	<b>76.76</b>	<b>61.65</b>
PV-RCNN	Base	85.98	54.43	16.49	86.28	80.79	72.37
	<b>Ours</b>	<b>89.48</b>	<b>62.47</b>	<b>31.13</b>	<b>90.43</b>	<b>85.89</b>	<b>40.21</b>
PartA2	Base	80.21	44.54	10.31	85.63	79.73	66.39
	<b>Ours</b>	<b>88.87</b>	<b>57.32</b>	<b>23.09</b>	<b>88.45</b>	<b>84.20</b>	<b>46.39</b>

Table 2. Comparison result with SOTA on KITTI Misc benchmark. 500 proposals are used for all cases.

Method	Recall @IOU			OOD detection		
	0.10	0.25	0.40	AUC	AP	FPR
Huang et al. [11]	76.70	44.74	18.14	70.55	62.37	85.57
<b>Ours (SECOND)</b>	81.65	48.87	26.60	88.48	82.94	55.05
<b>Ours (PointPillars)</b>	82.89	54.85	26.60	83.79	76.76	61.65
<b>Ours (PV-RCNN)</b>	<b>89.48</b>	<b>62.47</b>	<b>31.13</b>	<b>90.43</b>	<b>85.89</b>	<b>40.21</b>
<b>Ours (PartA2)</b>	88.87	57.32	23.09	88.45	84.20	46.39

#### 4.2.3 Comparison with SOTA

To the best of our knowledge, [11] is the only existing work on OOD classification for 3D object detector. Therefore, for a comparison with state-of-the-art (SOTA), we compare [11] using MSP, which shows the best or competitive performance across all datasets. Following [11], we leverage a PointPillars detector for Huang et al. [11]. Table 2 demonstrates the comparison between [11] and our method, in terms of metrics on both unseen object localization and OOD classification. Our method outperforms [11] with large margins across all evaluation metrics, irrespec-

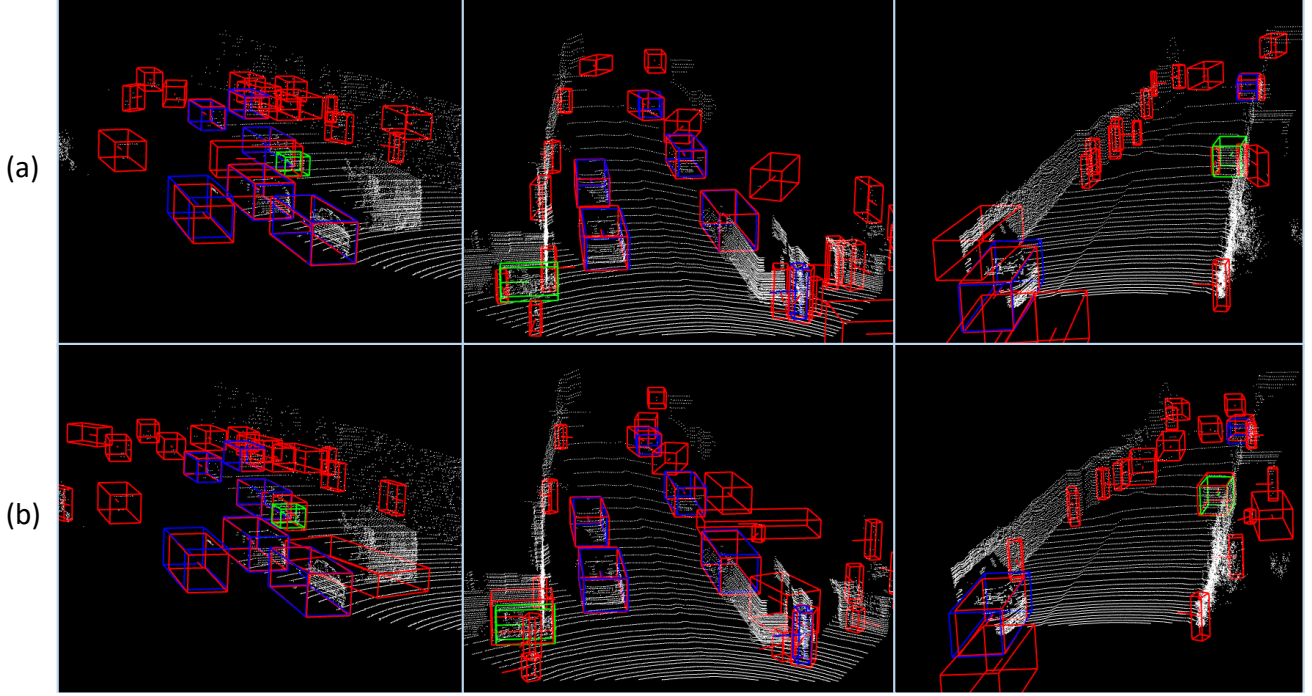


Figure 6. **Qualitative result of our method on KITTI Misc benchmark.** (a): Base detector result; (b): Our result.

tive of the backbone network.

#### 4.2.4 Qualitative Result

We qualitatively validate our method through visualization, specifically against the baseline SECOND detector. As shown in Figure 6, the top images depict the results of the conventional SECOND, while the bottom images showcase our method. Blue boxes represent ground truth boxes for in-distribution, and green boxes represent ground truth boxes for Misc. The red boxes indicate the Top-25 results from the final detection. In contrast to the baseline, which estimates unseen object 'Misc' localization with significantly different-sized boxes, our method consistently provides more accurate estimates with boxes of similar sizes. The superiority of our approach is visually evident, confirming its effectiveness.

### 4.3. Evaluation on Nuscenes OOD benchmark

#### 4.3.1 Comparison with baseline

We validate our method on the Nuscenes OOD benchmark, which comprises unseen objects in large-scale outdoor scenes not present in the outdoor KITTI dataset. We constructed a total of five benchmarks by introducing five OOD objects from Nuscenes to the KITTI scene. We select five OOD (unseen) object classes: Debris (Deb), Pushable Pullable Object (PPO), Traffic Barrier (TB), Traffic Cone (TC), and Animal (Ani). These objects are nearly unseen

Table 3. Quantitative result of our method (SECOND) on Nuscenes OOD benchmark.

Class	Method	Recall @IOU			OOD detection		
		0.10	0.25	0.40	AUC $\uparrow$	AP $\uparrow$	FPR $\downarrow$
Deb	Base	28.63	11.37	3.14	86.95	86.20	65.69
	<b>Ours</b>	<b>43.61</b>	<b>31.83</b>	<b>14.54</b>	<b>95.41</b>	<b>96.05</b>	<b>28.29</b>
PPO	Base	21.51	16.28	7.17	91.41	92.86	55.23
	<b>Ours</b>	<b>26.59</b>	<b>22.35</b>	<b>12.91</b>	<b>95.04</b>	<b>94.98</b>	<b>31.98</b>
TB	Base	23.03	1.62	0.40	88.29	86.39	59.39
	<b>Ours</b>	<b>36.49</b>	<b>22.78</b>	<b>14.31</b>	<b>96.13</b>	<b>95.82</b>	<b>21.77</b>
TC	Base	29.73	20.66	7.92	89.42	90.77	63.51
	<b>Ours</b>	<b>36.80</b>	<b>26.98</b>	<b>11.37</b>	<b>94.79</b>	<b>94.95</b>	<b>38.54</b>
Ani	Base	16.83	2.10	0.00	90.73	91.64	61.38
	<b>Ours</b>	<b>38.00</b>	<b>17.08</b>	<b>4.03</b>	<b>95.93</b>	<b>95.55</b>	<b>26.30</b>

objects in KITTI scenes. We introduce these OOD (unseen) objects on KITTI scenes by copy-pasting the point cloud data in the Nuscenes dataset. As shown in Table 3, our method on SECOND (SEC) outperformed the baseline in all five benchmarks. Similar results are obtained for PointPillars, PV-RCNN, and PartA2. We include all results in the supplementary.

### 4.4. Evaluation on SUN-RGBD OOD benchmark

#### 4.4.1 Comparison with baseline

We validate our method on the SUN-RGBD OOD benchmark, which consists of unseen objects in indoor scenes not present in the outdoor KITTI dataset (also, as a training sample). As summarized in Table 4, conventional base detectors struggle with detecting unseen objects that are syn-

Table 4. Quantitative result of our method on SUN-RGBD OOD benchmark.

METHOD		Recall @IOU			OOD detection		
		0.10	0.25	0.40	AUC↑	AP↑	FPR↓
SECOND	Base	69.40	25.28	2.44	84.63	85.99	85.81
	<b>Ours</b>	<b>92.36</b>	<b>66.97</b>	<b>34.16</b>	<b>96.94</b>	<b>96.96</b>	<b>9.44</b>
PointPillars	Base	67.69	22.49	3.93	76.23	74.49	93.65
	<b>Ours</b>	<b>85.56</b>	<b>47.63</b>	<b>23.49</b>	<b>90.28</b>	<b>87.46</b>	<b>32.97</b>
PV-RCNN	Base	80.27	24.22	2.02	90.58	88.62	50.67
	<b>Ours</b>	<b>97.33</b>	<b>79.33</b>	<b>43.56</b>	<b>96.25</b>	<b>96.55</b>	<b>5.12</b>
PartA2	Base	73.97	21.91	1.95	87.37	84.40	57.92
	<b>Ours</b>	<b>96.05</b>	<b>70.18</b>	<b>37.06</b>	<b>96.33</b>	<b>97.55</b>	<b>5.70</b>

thetically introduced from indoor scenes. Consistent with the results from the Misc benchmark, high-performance two-stage detectors outperform single-stage detectors in OOD classification. Furthermore, applying our method to all four detectors substantially improves unseen object detection and enhances OOD classification performance. This trend holds across all detectors.

## 5. Discussion

### 5.1. Effect of objectness node

We train the classification score used in object detection and the objectness score used in localization separately. In the inference phase, comparing our objectness score with the traditional confidence score, as summarized in Table 5, which confirms that our method achieves better performance in terms of localization.

Table 5. Effect of using objectness node.

METHOD	Objectness node	Recall @IOU		
		0.10	0.25	0.40
<b>Ours (SECOND)</b>	<b>X</b>	78.97	47.01	22.06
	<b>✓</b>	<b>81.65</b>	<b>48.87</b>	<b>24.12</b>

### 5.2. Comparison of OOD score metric

We obtain OOD classification performance for all baselines using the Energy score metric. Table 6 summarizes AUROC results obtained for various score metrics on the existing baseline. It can be observed that the choice of OOD score metric has a limited impact on 3D object detectors. The Energy score, while not necessarily the best, consistently demonstrates stable OOD performance across detectors.

### 5.3. Ablation study on augmentation method

We significantly improve unseen object detection performance by employing Multi-size Mix (MM) augmentation in conjunction with the Anomaly Sample (AS) augmentation obtained from indoor scenes. As summarized in Table 7, the combination of both augmentations yields the best-unseen object detection performance.

Table 6. Comparison of OOD score metric.

Metric	Method (AUROC↑)			
	SECOND	PointPillars	PV-RCNN	Part-A2
Max Logit [10]	85.54	75.37	86.28	85.66
Sum Logit [24]	85.65	<b>76.07</b>	<b>86.36</b>	83.56
Max Prob [24]	85.54	75.37	86.28	85.66
Sum Prob [24]	85.53	75.38	86.28	85.63
MSP [8]	<b>86.14</b>	70.55	85.52	<b>86.20</b>
Max Energy [24]	85.54	75.37	86.28	85.66
JointEnergy [24]	85.53	75.38	86.28	85.63
Energy [17]	85.53	75.38	86.28	85.63

Table 7. Augmentation method ablation result.

METHOD	Augmentation method		Recall @IOU		
	AS aug.	MM aug.	0.10	0.25	0.40
<b>Ours (SECOND)</b>	<b>X</b>	<b>X</b>	69.69	35.67	9.28
	<b>✓</b>	<b>X</b>	72.16	40.62	17.11
	<b>✓</b>	<b>✓</b>	<b>81.65</b>	<b>48.87</b>	<b>24.12</b>

## 5.4. Ablation study on loss

To enhance OOD classification performance, we incorporate additional losses, namely energy loss and contrastive loss. As summarized in Table 8, the use of contrastive loss significantly improves the separability between ID and OOD objects in feature embeddings, leading to a substantial enhancement in OOD classification performance compared to conventional methods.

Table 8. Loss component ablation result.

METHOD	Loss component		OOD detection		
	Energy	Contrastive	AUC↑	AP↑	FPR↓
<b>Ours (SECOND)</b>	<b>X</b>	<b>X</b>	85.53	81.17	78.14
	<b>✓</b>	<b>X</b>	86.38	79.13	58.35
	<b>✓</b>	<b>✓</b>	<b>88.48</b>	<b>82.94</b>	<b>55.05</b>

## 6. Conclusion

We introduce an integrated protocol for evaluating open-world 3D object detection on KITTI scenes, providing baseline assessments for four 3D object detectors: SECOND, PointPillars, PV-RCNN, and PartA2. By applying practical techniques to enhance the performance of existing 3D object detectors, we improve open-world 3D object detection performance in both unseen object detection and OOD classification. Additionally, by constructing three benchmark scenarios to model a diverse range of unseen objects, we confirm significant improvements in our method over baselines. We believe our work suggests a future direction for 3D object detectors in open-world scenarios, focusing on enhancing the detection and classification of unseen objects.

## References

- [1] Holger Caesar, Varun Bankiti, Alex H Lang, Sourabh Vora, Venice Erin Liong, Qiang Xu, Anush Krishnan, Yu Pan, Giancarlo Baldan, and Oscar Beijbom. nuscenes: A multimodal dataset for autonomous driving. In *Proceedings of the IEEE/CVF conference*



- on computer vision and pattern recognition, pages 11621–11631, 2020. 2, 5
- [2] Jun Cen, Peng Yun, Junhao Cai, Michael Yu Wang, and Ming Liu. Open-set 3d object detection. In *2021 International Conference on 3D Vision (3DV)*, pages 869–878. IEEE, 2021. 1, 3
- [3] Hyunjun Choi, JaeHo Chung, Hawook Jeong, and Jin Young Choi. Three factors to improve out-of-distribution detection. *arXiv preprint arXiv:2308.01030*, 2023. 5
- [4] Xuefeng Du, Xin Wang, Gabriel Gozum, and Yixuan Li. Unknown-aware object detection: Learning what you don’t know from videos in the wild. In *Proceedings of the IEEE/CVF Conference on Computer Vision and Pattern Recognition*, pages 13678–13688, 2022. 1, 2, 4
- [5] Xuefeng Du, Zhaoning Wang, Mu Cai, and Yixuan Li. Vos: Learning what you don’t know by virtual outlier synthesis. *arXiv preprint arXiv:2202.01197*, 2022. 1, 2, 4
- [6] Andreas Geiger, Philip Lenz, and Raquel Urtasun. Are we ready for autonomous driving? the kitti vision benchmark suite. In *2012 IEEE conference on computer vision and pattern recognition*, pages 3354–3361. IEEE, 2012. 1, 2, 3, 6
- [7] Ross Girshick. Fast r-cnn. In *Proceedings of the IEEE international conference on computer vision*, pages 1440–1448, 2015. 4
- [8] Dan Hendrycks and Kevin Gimpel. A baseline for detecting misclassified and out-of-distribution examples in neural networks. *International Conference on Learning Representations (ICLR)*, 2017. 3, 4, 8
- [9] Dan Hendrycks, Mantas Mazeika, and Thomas Dietterich. Deep anomaly detection with outlier exposure. *arXiv preprint arXiv:1812.04606*, 2018. 2, 4
- [10] Dan Hendrycks, Steven Basart, Mantas Mazeika, Mohammadreza Mostajabi, Jacob Steinhardt, and Dawn Song. Scaling out-of-distribution detection for real-world settings. *arXiv preprint arXiv:1911.11132*, 2019. 8
- [11] Chengjie Huang, Vahdat Abdelzad, Christopher Gus Mannes, Luke Rowe, Benjamin Therien, Rick Salay, Krzysztof Czarnecki, et al. Out-of-distribution detection for lidar-based 3d object detection. In *2022 IEEE 25th International Conference on Intelligent Transportation Systems (ITSC)*, pages 4265–4271. IEEE, 2022. 1, 3, 4, 6
- [12] KJ Joseph, Salman Khan, Fahad Shahbaz Khan, and Vineeth N Balasubramanian. Towards open world object detection. In *Proceedings of the IEEE/CVF conference on computer vision and pattern recognition*, pages 5830–5840, 2021. 1, 2
- [13] Prannay Khosla, Piotr Teterwak, Chen Wang, Aaron Sarna, Yonglong Tian, Phillip Isola, Aaron Maschinot, Ce Liu, and Dilip Krishnan. Supervised contrastive learning. *Advances in neural information processing systems*, 33:18661–18673, 2020. 5
- [14] Dahun Kim, Tsung-Yi Lin, Anelia Angelova, In So Kweon, and Weicheng Kuo. Learning open-world object proposals without learning to classify. *IEEE Robotics and Automation Letters*, 7(2):5453–5460, 2022. 1, 2, 3
- [15] Alex H Lang, Sourabh Vora, Holger Caesar, Lubing Zhou, Jiong Yang, and Oscar Beijbom. Pointpillars: Fast encoders for object detection from point clouds. In *Proceedings of the IEEE/CVF conference on computer vision and pattern recognition*, pages 12697–12705, 2019. 1, 2, 3
- [16] Tsung-Yi Lin, Priya Goyal, Ross Girshick, Kaiming He, and Piotr Dollár. Focal loss for dense object detection. In *Proceedings of the IEEE international conference on computer vision*, pages 2980–2988, 2017. 4
- [17] Weitang Liu, Xiaoyun Wang, John Owens, and Yixuan Li. Energy-based out-of-distribution detection. *Advances in Neural Information Processing Systems*, 33: 21464–21475, 2020. 3, 5, 8
- [18] Charles R Qi, Or Litany, Kaiming He, and Leonidas J Guibas. Deep hough voting for 3d object detection in point clouds. In *proceedings of the IEEE/CVF International Conference on Computer Vision*, pages 9277–9286, 2019. 4, 6
- [19] Kuniaki Saito, Ping Hu, Trevor Darrell, and Kate Saenko. Learning to detect every thing in an open world. In *European Conference on Computer Vision*, pages 268–284. Springer, 2022. 1, 2
- [20] Shaoshuai Shi, Zhe Wang, Xiaogang Wang, and Hongsheng Li. Part-a<sup>2</sup> net: 3d part-aware and aggregation neural network for object detection from point cloud. *arXiv preprint arXiv:1907.03670*, 2(3), 2019. 1, 2, 3
- [21] Shaoshuai Shi, Chaoxu Guo, Li Jiang, Zhe Wang, Jianping Shi, Xiaogang Wang, and Hongsheng Li. Pv-rnn: Point-voxel feature set abstraction for 3d object detection. In *Proceedings of the IEEE/CVF conference on computer vision and pattern recognition*, pages 10529–10538, 2020. 1, 2, 3
- [22] Shuran Song, Samuel P Lichtenberg, and Jianxiong Xiao. Sun rgb-d: A rgb-d scene understanding benchmark suite. In *Proceedings of the IEEE conference on computer vision and pattern recognition*, pages 567–576, 2015. 2, 4, 5, 6
- [23] OpenPCDet Development Team. Openpcdet: An open-source toolbox for 3d object detection from

- point clouds. <https://github.com/open-mmlab/OpenPCDet>, 2020. 6
- [24] Haoran Wang, Weitang Liu, Alex Bocchieri, and Yixuan Li. Can multi-label classification networks know what they don’t know? *Advances in Neural Information Processing Systems*, 34:29074–29087, 2021. 8
- [25] Kelvin Wong, Shenlong Wang, Mengye Ren, Ming Liang, and Raquel Urtasun. Identifying unknown instances for autonomous driving. In *Conference on Robot Learning*, pages 384–393. PMLR, 2020. 1
- [26] Yan Yan, Yuxing Mao, and Bo Li. Second: Sparsely embedded convolutional detection. *Sensors*, 18(10): 3337, 2018. 1, 2, 3
- [27] Yin Zhou and Oncel Tuzel. Voxelnet: End-to-end learning for point cloud based 3d object detection. In *Proceedings of the IEEE conference on computer vision and pattern recognition*, pages 4490–4499, 2018. 3

# UOD: Unseen Object Detection in 3D Point Cloud

## Supplementary Material

Our supplementary material covers the following topics:

**Algorithm Details for OOD Classification Evaluation:** Algorithm 1

**Nuscenes OOD Benchmark Full Result:** Table 9 and 10

**Implementation Details:** Specifics of our implementation process, including detailed training, hyperparameter tuning, and implementation details for baseline and our method.

**Original 3D Object Detection Results:** Due to spatial constraints in the main text, we provide a result of the original 3D object detection performance. Specifically, we present a comparison of the 3D object detection performance between the baseline model and our algorithm.

**More Visualization of Result on KITTI Misc Benchmark:** To supplement what couldn't be covered in the main text due to space limitations, we present additional visualization results for the KITTI Misc benchmark.

**Visualization of Result on Synthetic OOD Benchmark:** To supplement what couldn't be covered in the main text due to space limitations, we provide visualization results for the synthetic benchmark.

**Limitations:** We qualitatively analyze the limitations of our approach through visualization. Specifically, we compare and analyze failure cases of our method of localizing unseen objects in the KITTI Misc benchmark with the baseline.

### 7. Algorithm Details for OOD Classification Evaluation

We perform Out-Of-Distribution (OOD) classification based on scalar scores obtained from the In-Distribution (ID) classification score and OOD classification score from the final detection results. The evaluation metrics include AUROC, FPR95, and AUPR. In general, when ground truth and detection results have overlap, we can match them to obtain classification scores for both ID and OOD. However, in practice, it is common to encounter situations where there is no overlap for OOD data. Therefore, for precise OOD classification evaluation, we propose a separate handling for such ground truth samples. We address cases where IOU is not available by matching the closest detection result based on Euclidean distance. Our method follows the existing Hungarian-based matching, providing the advantage of avoiding heuristic parameter selection. As outlined in Algorithm 1, we first distinguish samples with no IOU and then handle them separately. For these cases, we perform matching based on distance to find the closest sample.

#### Algorithm 1: Hungarian Based Matching

---

**Input:**  $G_i$ : Ground truth  $M$ ,  $O_j$ : Detection results  $N$   
**Output:**  $M_i$ : Matching index result  
**Step0: Classify into results with overlap or no**  
 Get IOU matrix  $IOU_{i,j} \leftarrow$  IOU between pairs  $(G_i, O_j)$   
**for**  $i = 1$  **to**  $M$  **do**  
   **if**  $IOU_{i,j}$  is all zero **then**  
     | Gather as  $A_i$   
   **else**  
     | Gather as  $B_i$   
**Step1: IOU based hungarian matching**  
 Get IOU matrix  $IOU_{i,j} \leftarrow$  IOU between pairs  $(B_i, G_j)$   
 Hungarian Matching  $IM_i$  which maximize  $IOU_{i,j}$   
 Remove matched result  $C_j \leftarrow G_j$   
**Step2: Distance based hungarian matching**  
 Get distance matrix  $DIST_{i,j} \leftarrow$  IOU between pairs  $(A_i, C_j)$   
 Hungarian Matching  $DM_i$  which minimize  $DIST_{i,j}$   
 Aggregate and get final matching result  $M_i \leftarrow IM_i, DM_i$

---

Table 9. Quantitative result of our method (PointPillars) on Nuscenes OOD benchmark.

Class	Method	Recall @IOU			OOD detection		
	PointPillars	0.10	0.25	0.40	AUC $\uparrow$	AP $\uparrow$	FPR $\downarrow$
Deb	Base	31.51	17.61	4.89	82.30	78.31	69.67
	<b>Ours</b>	<b>38.60</b>	<b>29.43</b>	<b>15.20</b>	<b>90.50</b>	<b>88.45</b>	<b>43.86</b>
PPO	Base	22.61	17.24	8.24	85.06	80.37	64.37
	<b>Ours</b>	<b>25.92</b>	<b>22.24</b>	<b>11.99</b>	<b>88.11</b>	<b>85.67</b>	<b>55.32</b>
TB	Base	17.76	2.00	0.40	85.17	79.73	64.87
	<b>Ours</b>	<b>27.33</b>	<b>11.54</b>	<b>8.50</b>	<b>89.81</b>	<b>84.42</b>	<b>47.37</b>
TC	Base	28.57	17.76	5.21	87.57	89.39	69.88
	<b>Ours</b>	<b>34.56</b>	<b>22.59</b>	<b>7.14</b>	<b>90.49</b>	<b>89.52</b>	<b>51.16</b>
Ani	Base	15.62	2.48	0.00	87.21	86.60	67.62
	<b>Ours</b>	<b>30.84</b>	<b>12.84</b>	<b>2.30</b>	<b>91.63</b>	<b>90.60</b>	<b>42.91</b>

### 8. Nuscenes OOD Benchmark Detailed Result

We validate our method on the Nuscenes OOD benchmark, which comprises unseen objects in large-scale outdoor scenes not present in the outdoor KITTI dataset. For detailed results, we show the comparison results for other detectors: PointPillars and PartA2. As shown in Table 9 and 10, our method on PointPillars and PartA2 also outperformed the baseline in all five benchmarks.

### 9. Implementation Details

#### 9.1. SUN-RGBD Dataset Details

- The in-door SUN-RGBD database formed for 3D object detection in previous research, consists of 10 classes: [chair, desk, table, bookshelf, bed, nightstand, dresser, sofa, toilet, bathtub]. Each class is composed of the following number of samples: [9279, 933, 2539, 204, 771, 293, 182, 706, 171, 67].
- For anomaly sample augmentation, we specifically use

Table 10. Quantitative result of our method (PartA2) on Nuscenes OOD benchmark.

Class	Method	Recall @IOU			OOD detection		
	PartA2	0.10	0.25	0.40	AUC $\uparrow$	AP $\uparrow$	FPR $\downarrow$
Deb	Base	36.94	15.91	1.96	70.06	59.75	69.55
	<b>Ours</b>	<b>45.88</b>	<b>33.14</b>	<b>15.29</b>	<b>93.77</b>	<b>95.46</b>	<b>41.57</b>
PPO	Base	24.32	13.32	3.67	60.66	52.54	81.66
	<b>Ours</b>	<b>28.71</b>	<b>19.08</b>	<b>10.02</b>	<b>92.08</b>	<b>94.13</b>	<b>53.95</b>
TB	Base	29.21	3.65	0.81	69.18	58.29	68.15
	<b>Ours</b>	<b>39.76</b>	<b>19.07</b>	<b>6.49</b>	<b>94.57</b>	<b>96.11</b>	<b>36.51</b>
TC	Base	23.51	8.67	1.73	62.79	55.12	87.09
	<b>Ours</b>	<b>30.38</b>	<b>14.04</b>	<b>5.58</b>	<b>91.43</b>	<b>93.58</b>	<b>62.12</b>
Ani	Base	20.31	1.53	0.00	70.60	59.72	66.86
	<b>Ours</b>	<b>42.26</b>	<b>17.02</b>	<b>4.97</b>	<b>94.53</b>	<b>95.97</b>	<b>34.61</b>

the classes [chair, desk, table, bookshelf, bed], which collectively have a total of 13,725 samples. On the other hand, the classes [nightstand, dresser, sofa, toilet, bathtub], with a total of 1,419 samples, are utilized for constructing the SUN-RGBD OOD benchmark.

## 9.2. Configuration Setting Details

- Firstly, let's supplement additional details regarding the training configuration that are not covered in the main text. We introduce an additional 'Anomaly' class, and in connection with this, unlike the original three sizes of anchor boxes [[3.9, 1.6, 1.56]], [[0.8, 0.6, 1.73]], [[1.76, 0.6, 1.73]], we configure nine additional anchor box sizes to handle various sizes of the 'Anomaly' class. For this 'Anomaly' class, the anchor rotation, anchor bottom height, and matched/unmatched thresholds are set identically to the original configuration of the Pedestrian class. Specifically, the additional 9 sizes of anchor boxes are as follows: [[1.76, 0.6, 0.87], [0.8, 0.6, 0.87], [3.9, 1.6, 0.78], [3.9, 1.6, 1.56], [5.15, 1.91, 2.19], [9.20, 2.61, 3.36], [15.56, 2.36, 3.53], [2.5, 1.24, 1.62], [1.06, 0.54, 1.28]].
- Next, following the original configuration of OpenPCDet, we set the batch size per GPU to 4 for SECOND, PointPillars, and PartA2, while for PV-RCNN, it is set to 2. The experiments are conducted in an environment equipped with eight Quadro RTX 5000 16GB GPUs.
- Furthermore, we present additional details regarding our dataset configuration, which are not covered in the main text. In addition to the ground-truth sample augmentation for the original baseline detector, we incorporate additional Anomaly sample augmentation. Specifically, we construct the Anomaly database by substituting only the location of KITTI database objects into the original SUN-RGBD Anomaly samples. Moreover, to perform Multi-size Mix augmentation in this process, we organize even-numbered samples as the original anomaly samples and odd-numbered samples as resized anomaly samples.
- From the constructed Anomaly database, we set the "filter by min point" to 5, consistent with the setting for the original ground-truth samples, and the copy-pasted "sam-

ple number" is set to 20 consistent with the original augmentation of Car ground-truth "sample number".

## 9.3. Hyperparameter Setting

- To supplement the detailed hyperparameter settings not covered due to space constraints in the main text, we delve into further details.
- Firstly, regarding loss parameters, we set  $\lambda_{en} = 1.0$  and  $\lambda_c = 1.0$  without fine-tuning for a basic configuration. We provide detailed explanations for both the energy loss and contrastive loss. In detection, the number of scenes processed as input is determined by the batch size. Within each scene, multiple ID objects and 'Anomaly' class objects are collected. For these collected ID (seen) objects and OOD (unseen) objects, we compute energy regularization loss and contrastive loss.
- For energy loss calculation  $E(x)$ , we calculate log-sum-exp for three classes excluding the 'Anomaly' class: Car, Pedestrian, and Cyclist. We set  $m_{in} = -6.0$  and  $m_{out} = -3.0$ .
- Regarding contrastive loss, we use  $\tau_c = 0.10$ , a commonly used value in traditional contrastive learning settings.
- Objectness loss is added with the same weight as the existing classification loss, introducing additional learning for the objectness node. It is trained to assign 1 for all foreground, including the 'Anomaly' class, and 0 for the rest.

## 9.4. Additional Network Details

- We introduce additional networks for the existing dense head network, each dedicated to the objectness node configuration and an embedding layer for contrastive embedding.
- Firstly, the existing classification node is composed of a  $1 \times 1$  convolution as follows:  
Conv2D [Input-channels, anchor-per-location  $\times$  number-of-classes].
- Our objectness node is configured with one node per anchor as follows: Conv2D [Input-channels, anchor-per-location].
- The contrastive embedding in our approach obtains contrastive features for each anchor. It is structured as Conv2D [Input-channels, anchor-per-location  $\times$  feature-size]. Here, we set the feature size to 64, considering GPU memory.
- The obtained contrastive embedding is L2 normalized and utilized for contrastive learning.

## 9.5. Synthetic Benchmark Construction Setting

- The synthetic benchmark employs copy-paste augmentation, similar to the actual training process, but tests on synthetically generated scenes. In practice, we modify the



Table 11. Detection 3D AP result of our method on the KITTI dataset.

METHOD		Car 3D AP (R40)			Pedestrian 3D AP (R40)			Cyclist 3D AP (R40)		
		Easy	Mod	Hard	Easy	Mod	Hard	Easy	Mod	Hard
SECOND	Base	91.26	81.52	78.57	57.88	51.84	47.58	83.14	66.29	61.94
	<b>Ours</b>	91.32	81.51	78.38	58.74	53.33	49.47	81.23	63.78	60.74
PointPillars	Base	88.76	78.71	75.67	55.53	49.56	44.93	80.03	61.45	57.19
	<b>Ours</b>	87.83	75.39	72.15	53.30	47.71	43.05	81.24	63.00	58.76
PV-RCNN	Base	92.95	85.16	82.41	69.04	60.60	54.97	91.68	71.90	67.31
	<b>Ours</b>	92.35	84.50	82.07	60.27	54.48	50.29	85.26	66.68	62.72
Part A2	Base	92.30	84.06	81.68	62.22	56.37	51.19	89.41	72.09	67.47
	<b>Ours</b>	92.74	84.43	82.18	66.10	57.68	52.12	89.83	70.71	66.65

existing dataset configuration for the inference process. The specific approach aligns with the previous anomaly sample augmentation, where we use a test split from SUN-RGBD to construct a separate synthetic database from training. To ensure a consistent benchmark setup, we perform random augmentation only once and save it for fixed and repeated use. For Nuscenes OOD benchmark, we use the original training Nuscenes database for augmentation.

- To balance the number of unseen object samples between the synthetic benchmark and the KITTI Misc benchmark, we set the copy-pasting number of synthetic samples to 1 for scenes with miscellaneous objects. Specifically, for these scenes, we remove all other foreground classes, including miscellaneous objects, from the existing validation set and insert the synthetically generated samples.
- Concerning the construction of the synthetic database, we use the KITTI ground truth database as the target object for NN grid sampling, with a slice number  $N = 5$ . Similarly, we construct the synthetic database by substituting only the location of KITTI database objects into the original SUN-RGBD samples(or, Nuscenes samples).
- Here as well, similar to the Misc benchmark, we select scenes with unseen objects within the range of 0-50m from the synthesized results for validation.

## 10. Original 3D Object Detection Results

We compare the original 3D object detection performance between the baseline and our approach. As shown in Table 11, our method exhibits only minor loss in detection AP compared to the baseline. The observed decrease in detection AP is similar to the trade-off between classification accuracy and OOD classification performance in the classification task. A major contributing factor is that our method assigns high confidence to unidentified foreground objects mixed in the scene, beyond in-distribution classes: Car, Pedestrian, and Cyclist. We leave further research to minimize the loss in the original detection AP as future work.

## 11. More Visualization of Result on KITTI Misc Benchmark

We address additional visualization results for the KITTI Misc benchmark that couldn't be covered due to space constraints. As shown in Figure 7, our approach demonstrates more precise localization for various positions and shapes of Misc objects compared to the baseline. We have further validated the effectiveness of our method across a diverse range of scenes.

## 12. Visualization of Result on Synthetic Benchmark

We present visualization results for the synthetic benchmark that couldn't be covered due to space constraints. The synthetic benchmark models a more diverse range of unidentified foreground objects in terms of size and shape compared to the traditional Misc benchmark. As depicted in Figure 8, our approach exhibits more precise localization for various positions and shapes of unidentified foreground objects compared to the baseline. We qualitatively validate the effectiveness of our method on the synthetic benchmark. Performing 3D detection and OOD classification for these unseen objects is an essential technology for ensuring the stability of real autonomous driving algorithms.

## 13. Limitations with Visualization

We aim to analyze the limitations of our method through visualization, which couldn't be covered due to space constraints. Specifically, we identify the shortcomings by showcasing failure cases in unseen object detection. As seen in Figure 9, similar to the base detector, our method also struggles with localizing large unseen objects. Additionally, there are challenges in accurately localizing unseen objects with occlusion. This is because such objects have sparse points and lack sufficient context. This is a common issue experienced by conventional 3D object detectors, and detecting large objects with sparse points and limited context remains a future research challenge.

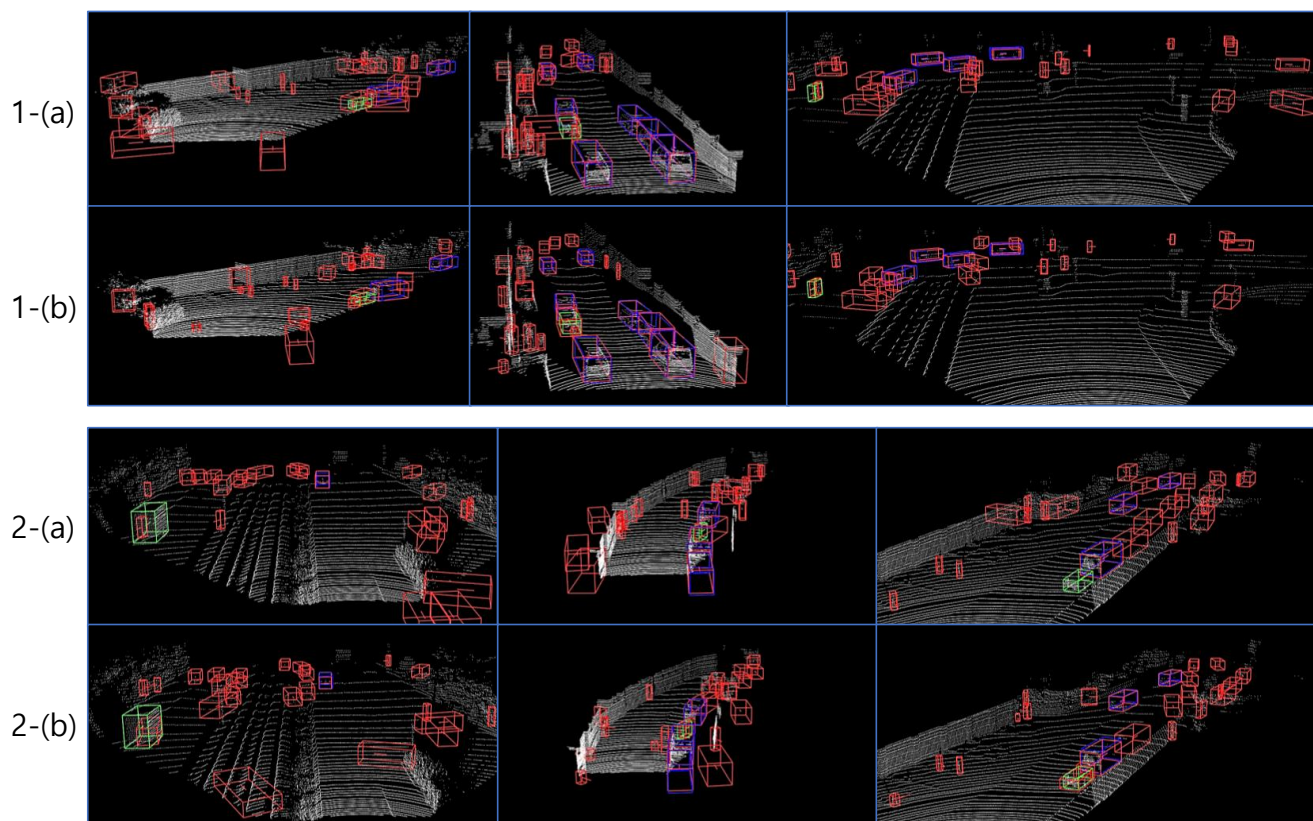


Figure 7. More Qualitative result of our method on KITTI Misc benchmark. (a): Base detector result; (b): Our result.

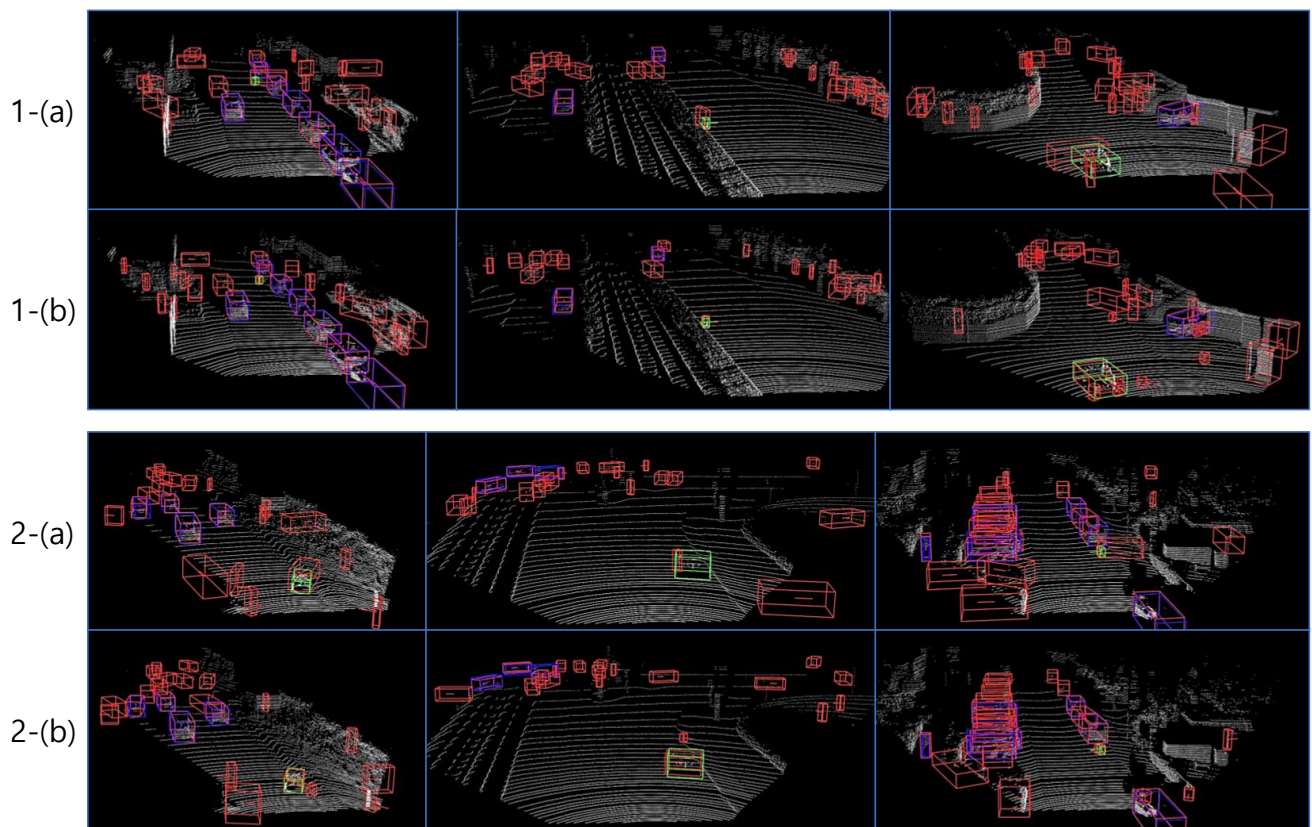


Figure 8. **Qualitative result of our method on sythetic benchmark.** (a): Base detector result; (b): Our result.

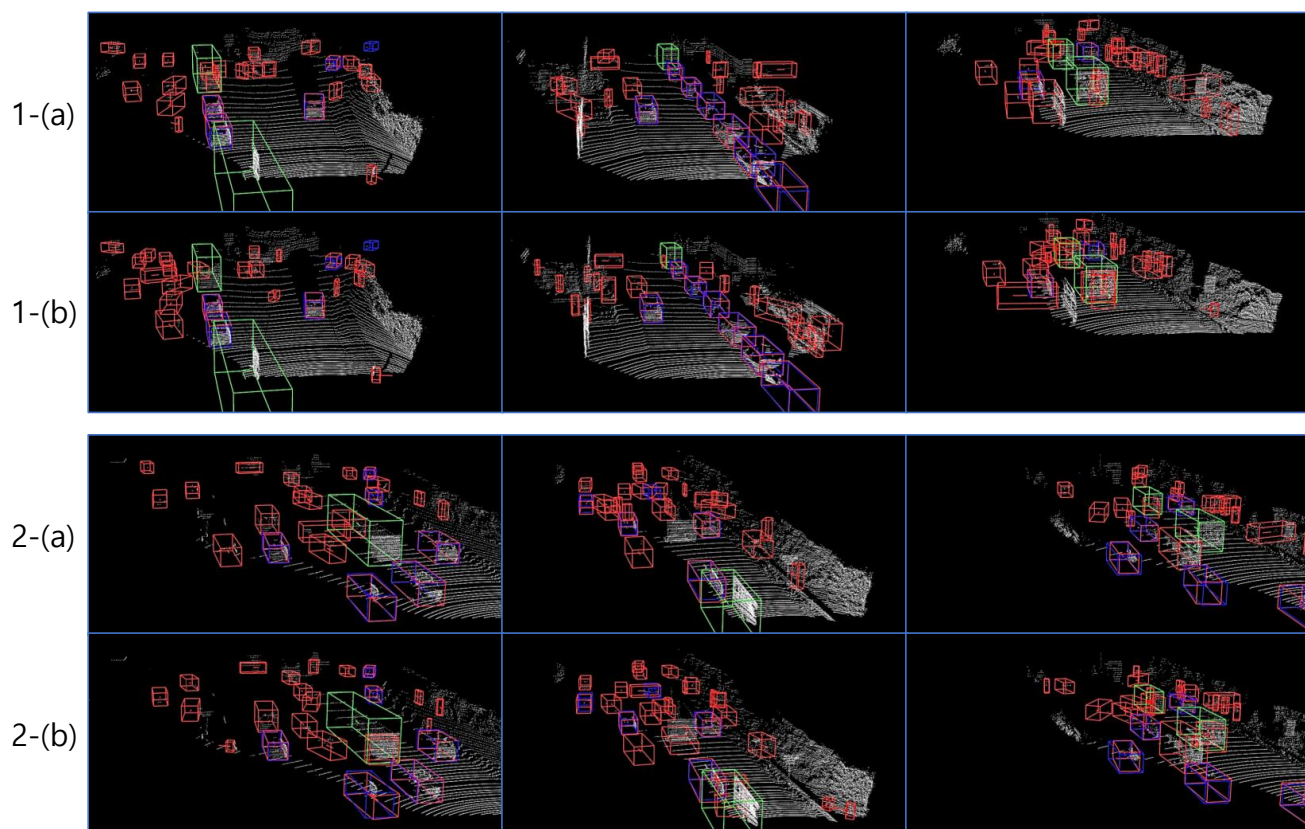


Figure 9. **Visualization result of failure case on KITTI Misc benchmark.** (a): Base detector result; (b): Our result.